CRITICAL INVESTIGATION OF MECHANICAL AND MICRO-STRUCTURAL PROPERTIES OF FRICTION STIR WELDED JOINTS OF AA-6061 T6

Ratnesh Kumar[1*],Bhabani Bora[2],Somnath Chattopadhyaya[2], Grzegorz Krolczyk[3]
[1]*Department of Mechanical Engineering, Indian Institute of Technology (ISM) Dhanbad-826004, India*
[1]*Department of Mechanical Engineering, Birla Institute of Technology, Mesra, Ranchi-835215, India*
[2]*Department of Mechanical Engineering, Indian Institute of Technology (ISM) Dhanbad, India*
[3]*Faculty of Mechanical Engineering, Opole University of Technology, Poland*
[*]*E-mail: ratan_876@yahoo.co.in*
Ph no.: +91-7549023950
Fax no.: 0326-2296563*r*

ABSTRACT*: In this study, effects of the process parameters on the mechanical and micro-structural properties of friction stir welded (FSW) joint of AA6061-T6 have been studied. Welding of aluminium alloy by conventional method is difficult. Therefore friction stir welding which is a solid state welding process, is emerging as a preferred method. After experimentation six samples were prepared at different process parameter i.e. rotational speed of 500, 710 and 1000 rpm along with welding speed of 25 and 40 mm/min. Tensile test and micro-hardness test were conducted on the samples to analyze the mechanical properties. Fractured surface of the tensile samples were also examined with field emission scanning electron microscope (FESEM). Microstructure of FSW joints were analysed with the help of optical microscopy (OM) as well as with FESEM. Different aspects of temperature development during the process were investigated using infrared thermal camera.*

KEYWORDS*:* Friction stir welding (FSW), AA-6061 T6, SS-410, Temperature, Tensile Strength, Microstructure, Micro-hardness.

1. INTRODUCTION

In the year 1991, the Welding Institute (UK) developed the friction stir welding (FSW) process [1]. Due to its clear industrial potential and many other advantages, this process has attracted attention of several industrial sectors, such as, aeronautics, transportation and automotive. The most significant advantage of the FSW process with respect to other processes is its ability to weld alloys that are difficult or impossible to join using fusion welding techniques. The FSW process takes place below the melting point of the material, i.e., in solid phase. Hence, it does not have the problems associated with re-solidification, such as, the formation of second phases, porosity, brittleness and cracking. Since it is a low-temperature process, it enables joining with lower distortion and lower residual stresses. Filler material or shielding gases are not required in this process. Therefore, it is energy-efficient as well. The other advantage compared to fusion welding is the fact that it does not generate fumes, arc flash, spatter and pollution [2]. Fig 1 shows the schematic drawing of friction stir welding.

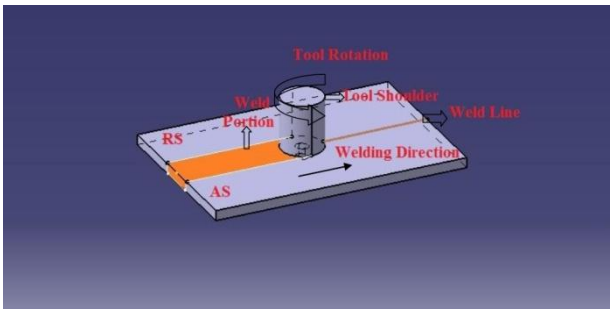

Fig 1 Schematic drawing of friction stir welding

2. LITERATURE REVIEW

Cavaliere et al. examined the effect of process parameters on mechanical and micro structural behaviour of AA6056 joints produced by FSW. They found that tensile strength and microhardness is maximum for highest welding and highest rotation speed [3]. Sakthivel et al. studied the effect of welding speed on mechanical and microstructural properties of FSW joint of commercial grade aluminium alloy. They concluded that best properties were obtained at lower welding speed [4]. Jayaraman et al. has characterized the effect of FSW process parameter on tensile strength, hardness and microstructure of A319 alloy welded

joint. They found the samples prepared at 1200 rpm rotational speed and 40 mm/min weld speed has superior properties compared to other samples [5]. Selvaraj M. et. al. conducted the experiments on 6mm thick AA6061-T6 plates. They use welding speed and rotational speed as welding parameters. They analysed different set of parameter for the sound weld. They observed that for a sound weld welding velocity and rotational speed has to be increase simultaneously. They also established a relation between process parameters, heat generated and formation of weld [6]. Zhang et. al. Used a thermo-mechanical model to study the effect of variation of shoulder size on material deformation during FSW. Through recrystallization formula, they proposed that the temperature variation is the main reason for grain growth near weld line. They found that temperature achieved can be increased with increase in shoulder diameter [7]. Kim et. al. numerically simulate plastic deformation and thermal history as well as microstructure evolution of FSW AA6111-T4. Using dislocation theory, the yield distribution was calculated at the weld zone [8]. Kim et. al. used the least square method to determine the relationship between the welding variables of FSW and the mechanical characteristics of the joint. They concluded that with increase in welding speed, tensile strength increases and hardness will be better at higher rotational speed [9]. Shojaeefard et. al. used 3D FEM analysis to investigate the effect of rotational and traverse speeds on peak temperature and heat affected zone (HAZ) width. The main outcome of their research is that with increasing rotational speed or decreasing traverse speed HAZ width increases with higher peak temperature [10]. Dehghani et. al analysed microstructural evolution and mechanical properties of FSW joints of aluminium alloy 7050-O. They observed better tensile and microhardness properties of welded joint with base metal. They found microstructural precipitates were coarser in the heat affected zone, while they are finer in the stirred zone [11]. Kang et al. used X-ray micrograph to study the material flow pattern inside the FSW plates. They concluded that on retreating side material flow is faster than that of advancing side [12]. Toktas et al. studied the effect of welding parameters on mechanical properties of friction stir welded AA6063-T4 plate having 3.7 mm thickness. They concluded that hardness value increased with rotation speed whereas yield and ultimate tensile strength were increases by the rotation speed at a low welding speed. All the tensile fracture occurred at the retreating side [13]. Yau et al used thermocouples to measure the temperatures distribution during the FSW process of AA2024-T3. They validate the welding temperature profile obtained experimentally using ANSYS model. They found good agreement between experimental thermal profiles with the results by the ANSYS model [14]. Krasnowski explained effect of tool shape on mechanical properties of AA 6082 FSW joint. They found a best mechanical property was obtained for FSW joints produced by a conventional and triflute tool [15]. Arora et al analysed the effect of process parameters on friction stir welding of aluminium alloy 2219-T87. They observed welding speed as most influential parameter for tensile strength and microstructure in nugget consisted of recrystallized grain structure [16]. Lim et al. examined tensile behaviours of friction stir welded joints obtained with different parameters. Based on two mechanisms i.e. increase in rotational speed and decrease in welding speed, increases the temperature and eventually decreases the strength. They found that tensile strength of these FSW alloys is not sensitive to process parameter [17]. Lafly et al. studied different properties of AA 6056 FSW welded samples. They observed large difference between the welded zone and base metal through hardness profile [18]. Mustafa et al used taguchi orthogonal array to design nine different tool shapes to study the effect on mechanical property of FSW T-joints for 3 mm AA6061-T6 without changing process parameter. They found optimal parameters for highest value of tensile strength [19]. Denquin et al. analyzed the micro-structural variations and properties of a friction stir welded joint of AA 6056. They discussed the influence of both thermal and mechanical cycles encountered during welding on this microstructural development [20]. Kamp et al. Applied a coupling model to predict the behaviour of FSW joints of 7050 alloys. Through the model they concluded that precipitate coarsening and dissolution under heating are the reason for strength variation[21]. Through their research Aval et al investigated the relationship between the thermo-mechanically affected zone and heat input in FSW of 5086 aluminium alloy. They concluded that peak temperature in advancing side is more than that of retreating side [22]. Azimzadegan and Serajzadeh studied the effect of weld parameters on 5 mm thick FSW joints of AA 7075-T6. They observed that with increase in rotational speed nugget zone's grain size reduced. They also suggested optimal rotational speed of tool for highest tensile strength [23]. Babu et al. developed a mathematical model with 95 % confidence level to find the tensile strength of FSW joints of AA2219. Their optimized values are closely matched with experimentally determined values [24]. Krasnowski investigated

the different properties of T-joints of EN-AW 6082-T6 produced by FSW process. He concluded that shape of fillet zones does not have significance influence on tensile strength [25]. Kim et al used thermo-mechanical simulations of friction stir spot welded joints. They analyzed material flow patterns using cylindrical pin and triangular pin. They also explain the flow pattern for the weld strength difference [26]. Sanders et al investigated microstructure and mechanical property of friction stir welded titanium alloy Ti-6Al-4V. They concluded that due to increase in hardness and grain refinement, fracture toughness increases [27]. Janjic M. et al carried out successful friction stir welding on aluminium alloy 6082-T6 having thickness 7.8 mm. They observed microstructure on advancing and retreating side is quite different. They observed sharp border between thermo-mechanically affected zone and stirred zone on advancing side and there is continuous change between the two regions on retreating side [28].

Now these days many researchers are studying theoretically and experimentally, the properties of friction stir welded joint of different alloys. The aim of this paper is to investigate experimentally the mechanical and microstructural properties of friction stir welded joint of 6 mm thick AA 6061 T6. In this experimental study temperature of FSW process is measured with the help of infrared camera.

3. EXPERIMENTAL PROCEDURE

3.1 Selection of material

The material used in this study was 6 mm thick plates of AA 6061 T6. The chemical composition of AA 6061 T6 is shown in table 1. The plates were cut into rectangular pieces of 150X50 mm. It is generally used in rail coaches, truck frames, ship building, civil bridges and military bridges, for aerospace applications, including helicopter rotor skins, etc.

Table 1 Nominal chemical composition of AA 6061

Contents	Cu	Fe	Si	Mn	Mg	Zn	Cr	Ti	Al
%	0.15-0.4	0.7	0.4-0.8	0.15	0.8-1.2	0.25	0.01-0.35	0.15	Rest

3.2 Selection of tool

The welding tool used was made of SS 410 stainless steel which has good corrosion resistance. Chemical composition of SS 410 is given in table 2.

Table 2 Chemical composition of SS 410

Contents	Cr	Mn	C	Ni	Mg	Fe
%	11.91	0.55	0.11	0.28	0.17	Balance

The tool had a shoulder portion and a tip portion. The diameter of the shoulder was 25 mm and the tip consisted of a cylindrical tapered profile with threads on it. The drawing of tool is shown in fig 2.

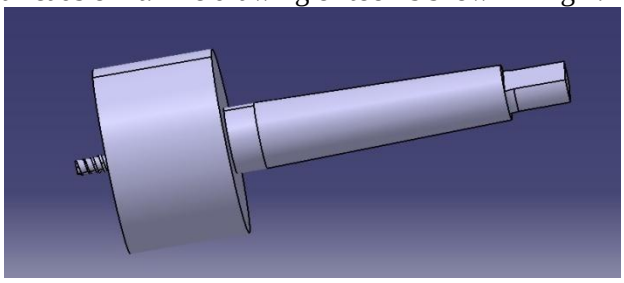

Fig 2 Drawing of tool

The dimensional nomenclature of tool is shown below.

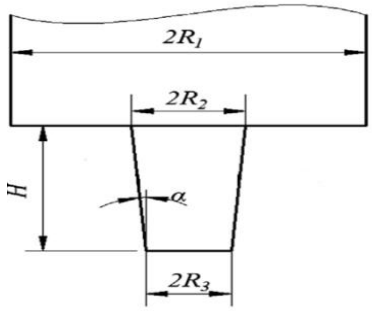

Fig 3 Shoulder and tip portion of tool

The dimensions corresponding to fig 3 are given below in table 3.

Table 3 Dimension of tool

Parameters	Vaue (mm)
Shoulder radius (R_1)	12.5
Pin top radius ($R_{2)}$	3.5
Pin bottom radius ($R_{3)}$	2.5
Height of pin (H)	5.7

The final figure of the tool is given in fig 4.

Fig 4 FSW tool

3.3 Experimental setup

The FSW experimental setup was developed on HMT 1U-make vertical milling machine. The tool was fixed on the tool post of a milling machine using tapered shank. The welding material was fixed on the milling bed using fixtures. A backing plate was used to support the weld between the milling bed and work-piece as shown in fig 5.

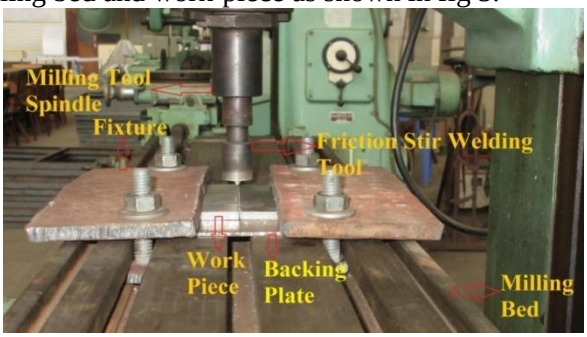

Fig 5 FSW experimental set-up

3.4 Selection of welding parameters

Welding speed and rotational speed of tool was selected as welding parameters. The experimentation was carried out at rotational speeds of 500 rpm, 710 rpm, 1000 rpm, respectively and at welding speeds of 25 mm/min and 40 mm/min. By using the above parameters, a total of six welding samples were prepared. Table 4 provides details regarding the process parameters used during the experimentation.

Table 4 Details of process parameters

Sr. No.	Sample no.	Tool rotational speed (rpm)	Welding speed (mm/min)
1.	1	500	25
2.	2	500	40
3.	3	710	25
4.	4	710	40
5.	5	1000	25
6.	6	1000	40

3.5 Testing procedure

Thermal images were taken with the help of infrared camera of CHAUVIN ARNOX C. A. 1888. These thermal images were then analysed with the help of RayCam reporting system software to get a reading of the maximum temperature and temperature distribution along the plate. Micro hardness was checked on Vicker microhardness tester, model no. MXT-70. The micro-hardness test was performed at a load of 100 gf for dwell time of 40 seconds and a distance of 1.25 mm interval across the weldment oriented transverse to the tool-path direction. Tensile test was performed to find the strength of the welded samples. The samples were prepared according to the ASTM E8 standards. The test was carried out on H50 KS, which was Hounsfield-make at a cross head speed of 10 mm/min and strain rate of 0.4 sec^{-1}. A fractured surface was observed with a field emission scanning electron microscope (FESEM). To study the micro-structure of the weldment, Keller's reagent (composition 95 ml water, 2.5 ml HNO3, 1.5 ml HCI, 1.0 ml HF) was used. Optical microscope and FESEM were used to evaluate the metallurgical characterization.

4. RESULT AND DISCUSSION

4.1 Temperature analysis

With the help of infrared camera, thermal images were taken at a regular interval to observe the temperature variations during the experiment. In fig 6, maximum temperature for sample 6 was read at 544.58^0 C, which was 80% of the melting temperature of the aluminium.

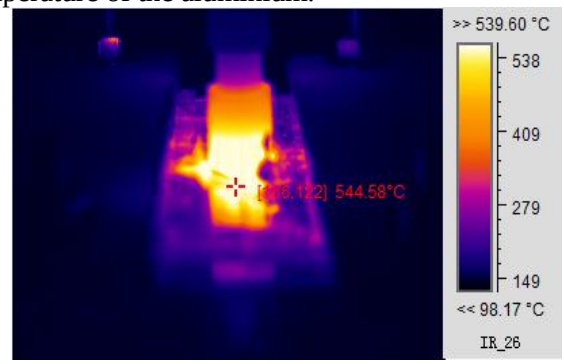

Fig 6 Maximum temperature during experimentation

Fig 7 (a) exhibits the thermal image of the experimental setup during the welding in which the advancing side and the retracting side of the weld can be seen. Fig 7 (b) exhibits the variation of temperature along the line drawn as shown in fig 7 (a). Vertical line in fig 7 (b) shows the central position of the weld. It can be clearly observed that the temperature of the advancing side (AS) is 10 - 20^0 C higher than that of the retreating side (RS) [19]. This is due to the fact cooler material from advancing side swept by the tool to the retreating side. Therefore temperature of advancing side increases and consequently reduces the temperature of retreating side.

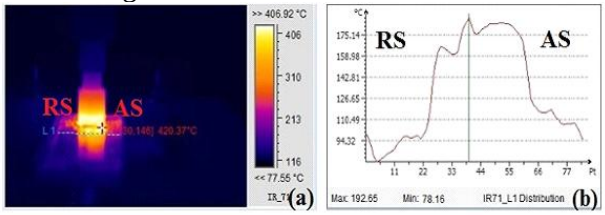

Fig 7 Variation of temperature at different points on plate along line as shown in (a)

During the welding process for all specimen, continuous temperature was recorded by IR camera. Fig 8 shows temperature variation in all the six

specimens with respect to time. From fig 8, it is clear that temperature starts increasing as process proceeds. After some time, it achieves the maximum temperature and remains constant through-out the process. It is observed that time required to achieve the maximum temperature level decreases with increase in rotational speed. From this study it is concluded that process takes 5 minutes for 500 rpm, 3 minutes for 710 rpm and 2 minutes at 1000 rpm to achieve maximum temperature limit as shown in figure 8.

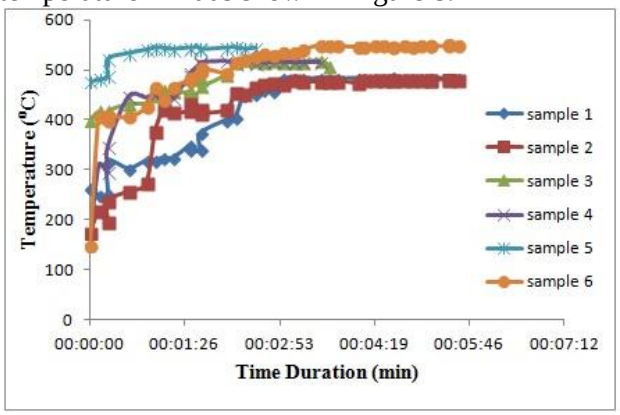

Fig 8 Time temperature graph for FSW process

4.1 Mechanical properties

4.1.1 Hardness test

Figure 9 shows the micro-hardness distribution along the cross section of the joints. Base material, i.e., AA6061, was in the range of 90-95 HV. The microhardness distribution profiles for all the six samples exhibited W-shape. As shown in fig 9, it is clear that hardness value is unaffected from the change in process parameter. For all the six cases, microhardness in the welded zone became reduced by 14% in contrast to the base material. The hardness of HAZ and TMAZ was observed lower than that of centre of weld i.e. nugget zone. At the centre of weld maximum hardness is observed. Outside this region, at TMAZ and HAZ it reduces slightly then towards base material it increases sharply as shown in figure 9. Due to overaging effect minimum hardness was observed at HAZ. Therefore, there is slight deformation in HAZ, which results in different thermo mechanical properties at nugget and THAZ. The formation of precipitates and fine grains are the reason for slight increase in hardness in the SZ compared to the HAZ and the TMAZ. At TMAZ of retreating side a slight hardness was observed as compared to that of advancing side. This was due to a broader temperature gradient resulting in overaging and less dissolution [29]. As per fig 9, hardness value in the nugget zone was of the order of 77-79 HV, and, in the HAZ, it was in the range of 64-66 HV.

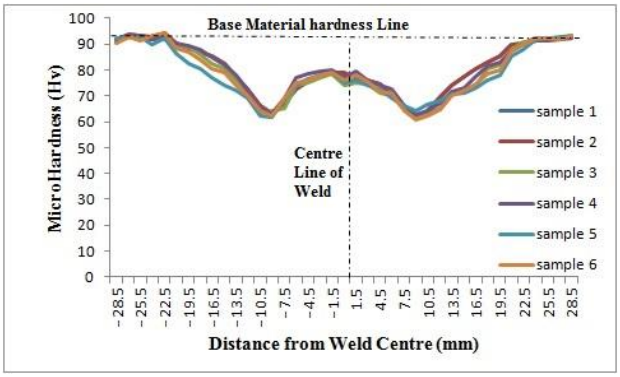

Fig 9 Microhardness distribution of all six welded joints

4.1.2 Tensile test

Tensile specimen was prepared as per ASTM E8 standards from all the six welded samples. [30]. Dimensional drawing of the tensile sample is shown in figure 10.

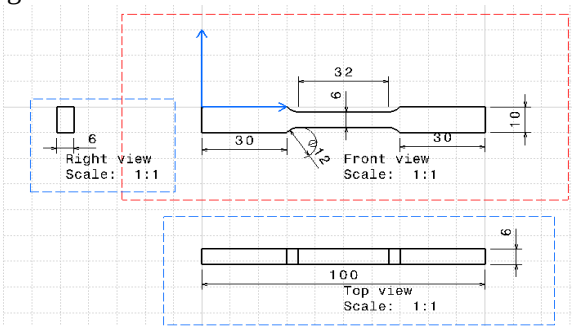

Fig 10 Tensile test specimen diagram

After the welding processes were complete, two samples for each welding joint were prepared for the tensile test. Below, figure 11 shows the cut cross-section of the welded section in the transverse direction of the welding. It can be observed in fig 11 that after friction stir welding, there was no surface defect, such as, like porosity or hole.

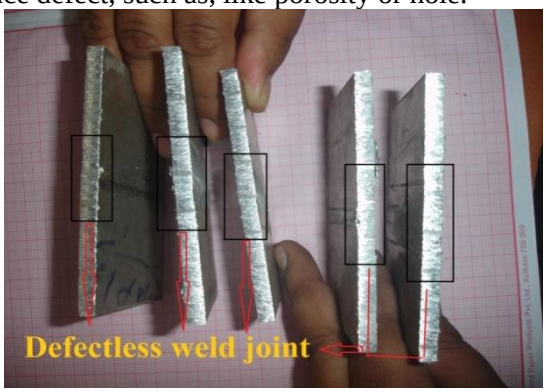

Fig 11 Cross-sectional image of Friction stir welded sample

Fig 12 shows one tensile specimen for each weld joint. Fig 12 (a) shows the tensile specimens before testing and fig 12 (b) shows the tensile specimens after test.

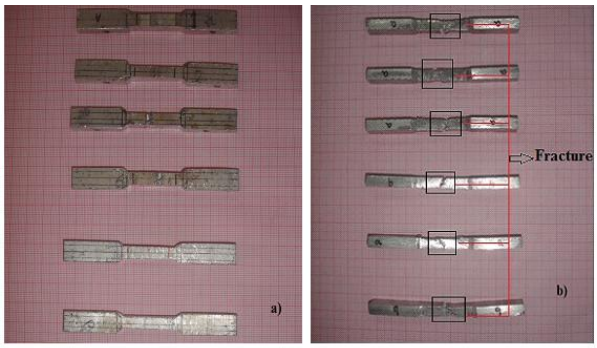

Fig 12 Tensile specimen a) before test, b) after test

As shown in figure 12 (b), during the tensile test, first, necking occurred at the lowest microhardness part till this part was completely fractured. The fracture developed at the lowest hardness area of the joint which is at the HAZ on advancing side adjacent to TMAZ as shown in figure 9. Figure 13 shows the force Vs extension graphs during the tensile test.

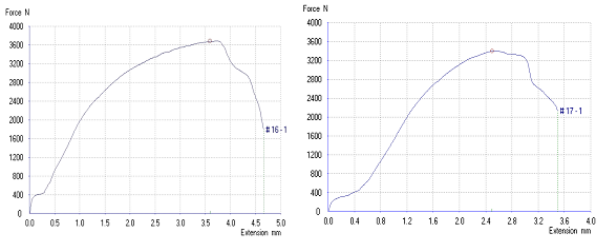

Fig 13 load versus elongation graph for sample no 1 & 2

After observing the force Vs extension graph in all the six samples, it can be concluded that the welded samples showed ductile behaviour. For each parameter two tensile specimens are tested and average of two specimens for ultimate tensile strength is presented in fig 14. The variation of the ultimate tensile strength (UTS) of the welded sample with reference to the rotational speed of the tool at 25 mm/min and 40 mm/min welding speed is shown in fig 14.

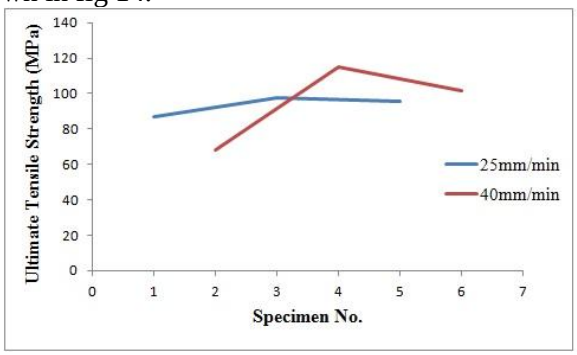

Fig 14 Variation of UTS with respect to process parameter

At constant welding speed, as tool rotational speed increases, UTS increases up to a maximum value. Further increase in tool rotational speed starts decreasing the UTS. As shown in fig 14 UTS is maximum at 710 rpm for both weld speed. From fig 14, it is clear that at 710 rpm, as welding speed increased from 25 mm/min to 40 mm/min, the UTS increased by 20.14%. Low friction is observed at lower rotational speed and higher welding speed due to which low heat is generated. Therefore, in the welded zone irregular mixing of material and poor plastic flow was observed. Hence, the UTS is low in case of sample 1 and 2. From fig 14, the lowest UTS can be observed at the lowest rotational speed, i.e., 500 rpm. The higher rotational speed and the lower welding speed produce sufficient heat for metallurgical phenomena, such as, grain coarsening, solubilisation and coarsening of strengthening precipitates at the weld zone. Therefore UTS value decreases due to lower dislocation density [31]. As, it can be observed, that UTS of sample 5 is 8.42 % less than that of sample 6. Percentage elongations in all the six welded specimens were in the range of 12-14%.

4.1.3 Fractured surfaces analysis

Tensile-tested specimens were analysed with FESEM to understand the fracture behaviour. Fig 15 and 16 show the FESEM images of the tensile-tested fractured surface of sample no. 1 and 2, respectively; while fig 15 (a) (top right), 15 (b) (bottom left), 15 (c) (bottom centre) and 15 (d) (bottom right) as well as fig 16 (a) (top right), 16 (b) (bottom left), 16 (c) (bottom centre) and 16 (d) (bottom right) show the magnified points marked in the image. In both cases large area of microscopic voids of different sizes and shapes is found A large number of dimples with different depths can be observed as well indicating formation of a ductile fracture in these regions [32]. Two types of dimples are observed; the first one is bigger and deeper as shown in fig 15 (b) (bottom left) and 15 (d) (bottom right) as well as in fig 16 (b) (bottom left) and 16 (d) (bottom right). Another type of dimple, which is smaller and shallower is shown in fig15 (a) (top right) and 15 (c) (bottom centre) as well as in fig 16 (a) (top right) and 16 (c) (bottom centre).

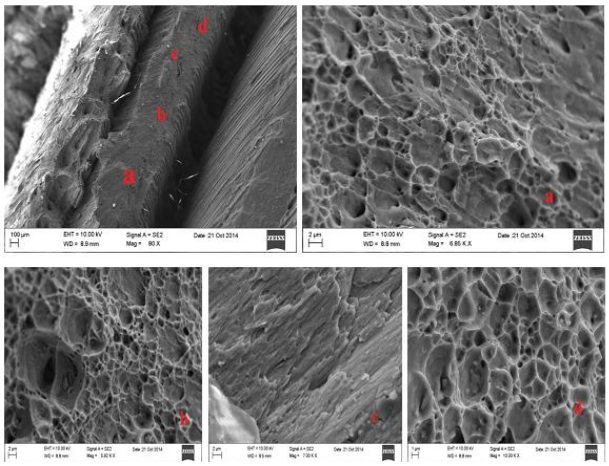

Fig 15 Fracture surface FESEM images for specimen no 1

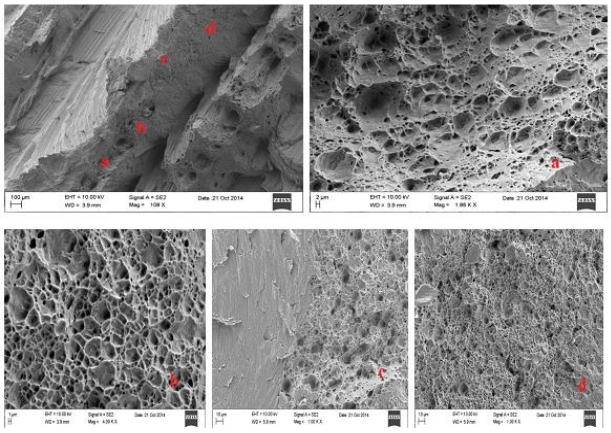

Fig 16 Fracture surface FESEM images for specimen no 2

4.2 Microstructural analysis

Microstructure of the base metal as well as friction stir welded samples can be observed with the help of optical microscopy and FESEM to study the micro-structural changes. Fig 17 shows the optical microscopy (OM) image of the base metal.

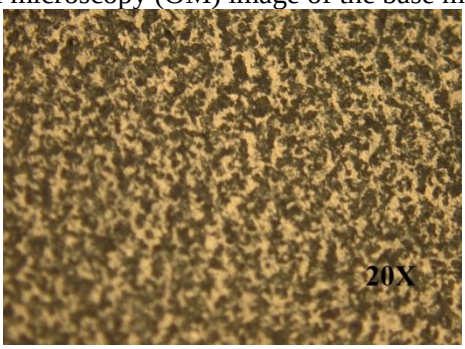

Fig 17 OM image of base metal

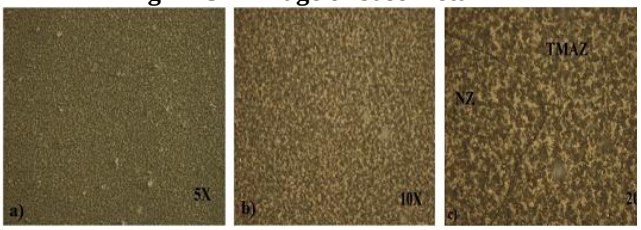

Fig 18 OM images of welded sample 3 at different magnification

Fig 18 shows optical microscope images of welded sample 3 at three different magnifications. Small grains was observed due to high plastic deformation and high temperature in the welded sample as compared to the base metal in figure 18. The initial elongated grains of the parent material were mechanically converted to new equi-axed fine grain structure as shown in fig 18 (a) and 18 (b). In fig 18 (c), nugget zone (NZ) and the thermo mechanically affected zone (TMAZ) can be easily distinguished.

Fig 19 shows the FESEM image of the welded sample no. 1 in which the nugget zone and thermo mechanically affected zone are visible. Fine and equi-axed grains of the nugget zone as compared to that of the thermo mechanically affected zone could be observed due to which hardness of the nugget zone was higher than the thermo mechanically affected zone.

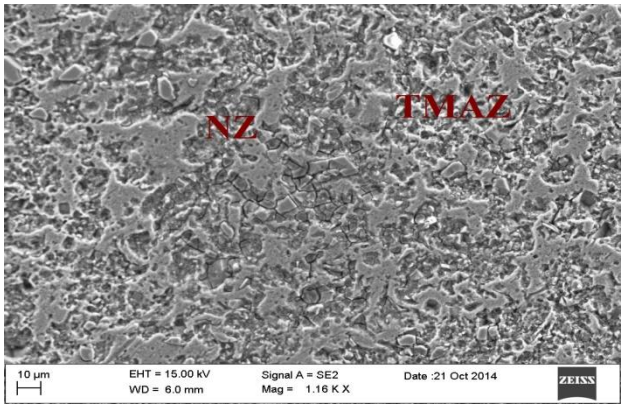

Fig 19 NZ and TMAZ for FS welded sample 1

At heat affected zone low temperature field was generated therefore, no re-crystallization occurs in this region [32]. Hence from figure 20, it could be observed that the grain dimension have considerably increased and the grains had less equi-axed character. As a result, hardness is low in heat affected zone compared to nugget zone and thermo mechanically affected zone.

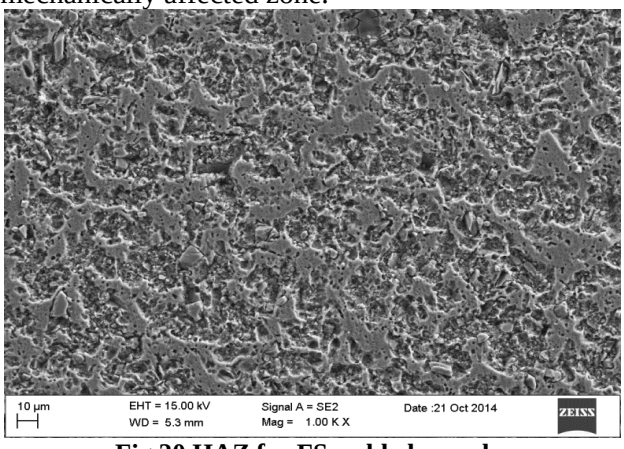

Fig 20 HAZ for FS welded sample

An EDX analysis was performed for the nugget region of friction stir welded joints to investigate the phases that were formed during welding process. Figure 21 shows EDX analysis of the FSW joint.

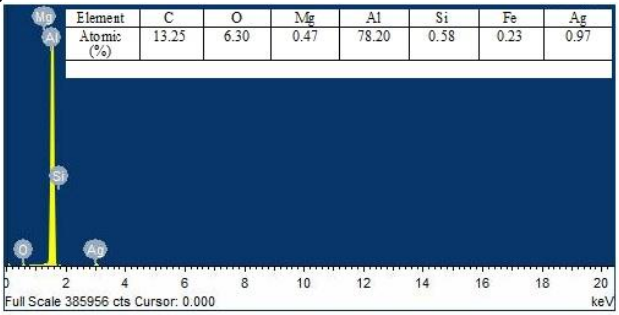

Fig 21 EDX images of nugget region of stir welded joints

From the EDX results as shown in fig 21 large percentage of carbon particles are confirmed. The presence of carbon in nugget region might be due diffusion of carbon atom from the welding tool during the friction stir welding process.

5. CONCLUSION

In this study, the focus has been on the mechanical and micro-structural behaviour of the friction stir welded joint of AA 6061 T6. The following conclusions can be drawn, based on the results of the experiments.

1. Tensile strength of the friction stir welded sample increases with an increase in rotational speed up to a certain level, i.e., up to 710 rpm. After that, it decreases.

2. With an increase in the welding speed from 25 mm/min to 40 mm/min, tensile strength can increase by 20% for particular rotational speeds.

3. Grain dimension in the HAZ region considerably increases; so, it has the lowest hardness value. Hence, it is the region of failure during the tensile test.

4. Temperature attained during the friction stir welding is 80% of the melting point of the material. The temperature of retreating side is $10\text{-}20^0$ C lower than that of the sdvsncing side. As rotational speed increases, time required to achieve peak temperature decreases.

6. References

(1) W.M. Thomas, E.D. Nicholas, J.C. Needham, M.G. Murch, P. Temple-Smith, C.J. Dawes, (1991) International Patent Application No. PCT/GB92/02203 and GB Patent Application No. 9125978.8 and US Patent Application No. 5,460,317.

(2) Gibson B. T., Lammlein D. H., Prater T. J., Longhurst W. R., Cox C. X.,Ballun M. C., Dharmaraj K. J., Cook G. E., Strauss A. M., (2004) Friction stir welding: process, automation and control, Journal of Manufacturing Processes 16, 56-73.

(3) Cavaliere P.,Campanile G.,Panella F.,Squillace A., (2006) Effect of welding parameters on mechanical and microstructural properties of AA 6056 joints produced by friction stir welding,Journal of Materials Processing Technology 180, 263-270.

(4). Sakthivel T., Sengar G. S., Mukhopadhyay J., (2009) Effect of welding speed on microstructure and mechanical properties of friction-stir-welded aluminium, International journal of advanced manufacturing Technology 43,468-473.

(5). Jayaraman M., Sivasubramanian R., Balasubramanian V., Babu S., (2009) Influence of process parameters on tensile strength of friction stir welded cast A319 aluminium alloy joints, Metals and materials international (15), 2, 313-320.

(6). Selvaraj M., Murali Vela, Rao Koteswara S. R., (2013) Mechanism of weld formation during friction stir welding of aluminium alloy, Materials and manufacturing Processes 28, 595-600.

(7). Zhang Z., Liu Y. L., Chen J. T., (2009) Effect of shoulder size on temperature rise and the material deformation in friction stir welding, International Journal of advanced Manufacturing Technology 45, 889-895.

(8). Kim Ji Hoon, Barlat Frederic, Kim Chongmin, Chung Kwansoo, (2009) Thermo-mechanical and microstructural modeling of friction stir welding of 6111-T4 aluminium alloys, Metals and Materials International (15) 1, 125-132.

(9). Kim Weon-Kyong, Won Si-Tae, Goo Byeong-Choon, (2010) A study on mechanical characteristics of the friction stir welded A6005-T5 extrusions, International Journal of Precision Engineering and Manufacturing (11), 6, 931-936.

(10). Shojaeefard Mohammad Hasan, Akbari Mostafa, Asadi Parviz, (2014) Multi objective optimization of friction stir welding parameters using FEM and neural networks, International Journal of Precision Engineering and Manufacturing (15) ,11, 2351-2356.

(11). Dehghani K., Ghorbani R., Soltanipoor A. R., (2015) Microstructural evolution and mechanical properties during the friction stir welding of 7075-O aluminium alloy, International Journal of advanced manufacturing Technology 77, 1671-1679.

(12). Kang Hoon Suk, Han Heung Nam, Oh Kyu Hwan, Cho Jae-Hyung, Lee Chang Gil, Kim Sung-Joon, (2009) Investigation of the material flow and texture evolution in friction-stir welded aluminium alloy, Metals and materials International (15), 6, 1027-1031.

(13). Toktas Alaaddin, Toktas Gulcan, (2012) Effect of welding parameters and aging process on the mechanical properties of friction stir welded 6063-T4 Al alloy, Journal of Materials Engineering and Performance 21 (6), 936-945.

(14). Yau Y. H., Hussain A., Lalwani R. K., Chan H. K., Hakimi N., (2013) Temperature distribution study during the friction stir welding process of Al2024-T3 aluminium alloy, International Journal of Minerals, Metallurgy and Materials 20 (8), 779-787.

(15). Krasnowski K., Hamilton C., Dymek S., (2015) Influence of the tool shape and weld configuration on microstructure and mechanical properties of the Al 6082 alloy FSW joints, Archieves of Civil and Mechanical Engineering 15 , 133-141.

(16). Arora Kanwer S., Pandey Sunil, Schaper Michael, Kumar Rajneesh, (2010) Effect of process parameters on friction stir welding of aluminium alloy 2219-T87, International Journal of advanced Manufacturing Technology 50, 941-952.

(17). Lim Sunggon, Kim Sangshik, Lee Chang-Gil, Kim Sung Joon, (2005) Mechanical properties of friction stir welded Al alloys with different hardening mechanisms, Metals and Materials International 11 (2), 113-120.

(18). Lafly A. L., Allehaux D., Marie F., Donne Dalle C., Biallas G., (2006) Microstructure and mechanical properties of the aluminium alloy 6056 welded by friction stir welding technique, Welding in the world, 50, 11/12, 98-106.

(19). Mustafa F. Faiz, Kadhym Ali H., Yahya Hiba H., (2015) Tool geometries optimization for friction stir welding of AA6061-T6 aluminium alloy T-joints using taguchi method to improve the mechanical behaviour, Journal of Manufacturing Science and Engineering 137, 1-8.

(20). Denquin A., Allehaux D., Campagnac M. H., Lapasset G., (2002) Relationship between microstructural variations and properties of a friction stir welded 6056 aluminium alloy, Welding in the world, 46, 11/12, 14-19.

(21). Kamp N., Reyonlds A. P., Robson J. D., (2009) Modelling of 7050 aluminium alloy friction stir welding, Science and Technology of Welding and Joining 14 (7), 589-596.

(22). Aval Jamshidi H., Serajzadeh S., Kokabi A. H., (2011) Theoretical and experimental investigation into friction stir welding of AA 5086, International Journal of Advanced Manufacturing Technology 52,531-544.

(23). Azimzadegan T., Serajzadeh S., (2010) An investigation into microstructures and mechanical properties of AA7075-T6 during friction stir welding at relatively high rotational speeds, Journal of Materials Engineering and Performance 19 (9), 1256-1263.

(24). Babu S., Elangovan K., Balasubramaniam V., Balasubramaniam M., (2009) Optimizing friction stir welding parameters to maximize tensile strength of AA 2219 aluminium alloy joints, Metals and Materials International 15 (2),321-330.

(25). Krasnowski K., (2014) Experimental study of FSW T-joints of EN-AW 6082-T6 and their behaviour under static loads, Arabian Journal of Science and Engineering 39, 9083-9092.

(26). Kim Dongun, Badrinarayan Harsha, Ryu Ill, Kim Hoon Ji, Kim Chongmin, Okamoto Kazutaka, Wagoner R. H., Chung Kwansoo, (2010) Numerical simulation of friction stir spot welding process for aluminium alloys, Metals and Materials International 16 (2),323-332.

(27). Sanders D. G., Edwards P., Cantrell A. M., Gangwar K., Ramulu M., (2015) Friction stir welded Titanium alloy Ti-6Al-4V:Microstructure, mechanical and fracture properties, The Journal of the Minerals, Metals and Materials Society 67 (5), 1054-1063.

(28). Janjic M., Vukcevic M., Mandic V., Pavletic D., Sibalic N., (2012) Microstructural evolution during friction stir welding of AlSi1MgMn alloy, Metalurgija 51(1), 29-33.

(29) Kumar R, Chattopadhyaya S, Hloch S, Krolczyk G, Legutko S. Wear characteristics and defects analysis of friction stir welded joint of aluminium alloy 6061-t6. Eksploatacja i Niezawodnosc – Maintenance and Reliability 2016; 18 (1): 128–135.

(30) *Annual Book of ASTM Standards*, section 3,vol 3.01 Metals –Mechanical Testing, Elevated and Low Temperature Tests, ASTM E8, 1983.

(31) Heidarzadeh A.,Khodaverdizadeh H., Mahmoudi A., Nazari E., (2012) Tensile behaviour of friction stir welded AA 6061-T4 aluminium alloy joints, Materials and design 37, 166-173.

(32) Cavaliere P., Nobile R.,Panella F. W., Squillace A., (2006) Mechanical and microstructural behaviour of 2024-7075 aluminium alloy sheets joined by friction stir welding ,International journal of machine tools & manufacture 46 , 588-594.